Optics Letters

Achromatization of conical diffraction: application to the generation of a polychromatic optical vortex

CLEMENT FALLET* AND GABRIEL Y. SIRAT

Bioaxial, ParisBiotech Santé, 24 rue du Faubourg Saint-Jacques, 75014 Paris, France
**Corresponding author: clement.fallet@bioaxial.com*

Received 22 December 2015; revised 18 January 2016; accepted 19 January 2016; posted 19 January 2016 (Doc. ID 256205); published 5 February 2016

Vortex beams are plagued by the intrinsic chromaticity of the physical phenomenon used to generate them. To the authors' best knowledge, attempts to generate them in a broad spectral range remain quite scarce and limited in their results. Crystal optics and especially conical diffraction (CD) (or refraction) intrinsically create achromatic vortices. The vortex is created by a wavelength-independent topological charge, embedded directly in the Fresnel equations. However, for biaxial crystals of low crystallographic symmetry, which includes all crystals used practically for CD, the dispersion of the binormal axis creates a chromaticity effect. In this Letter, we propose a new way to compensate this dispersion of the binormal axis of a biaxial crystal in order to generate white-light vortex beams by CD in a 250 nm spectral range, covering almost all the visible range. The advantages of the ability to use CD in a wide spectral range vastly exceed the sole generation of vortex beams.

OCIS codes: (050.4865) Optical vortices; (220.1000) Aberration compensation; (260.1180) Crystal optics; (260.6042) Singular optics.

http://dx.doi.org/10.1364/OL.41.000769

Optical vortex beams have gained much interest in recent years especially for their use in optical trapping [1] and for depletion of fluorescence in stimulated emission depletion (STED) microscopy [2]. The most common approaches to generating an optical vortex are a spiral phase plate [3] and computer generated holograms (CGH) [4]. However, these techniques intrinsically highly depend on the incoming wavelength, since they rely on a specific phase change and thus can only operate in a very narrow bandwidth. To the authors' best knowledge, Swartzlander's work is one of the only successful attempts to generate achromatic optical vortices [5] on a 100 nm range, thanks to the combination of two materials whose interface resembles a helicoid. Vortex creation by conical diffraction (CD) differs intrinsically from other means; the singularity is embedded in the Fresnel equations of the media as a topological feature and the zero arises both from a phase singularity and a zero of amplitude in the pupil plane. Though a pretty exotic phenomenon predicted in 1832 [6], CD has been at the center of many interesting papers published in recent years in domains ranging from optical trapping [7], laser amplification [8], polarimeter design [9], to superresolution microscopy [10,11].

We remind the reader briefly of the CD parameters and, explicitly, their wavelength dependency. A thorough and exhaustive introduction to CD and the origins of the equations presented here can be found in the seminal articles of Sir Berry [12,13], which are a clarification of the theory formerly developed by Belskii and Khalpalyuk [14].

For a biaxial crystal, assuming that x, y, z are the principal axes of the dielectric tensor, the orientation of the binormal optic axis β with respect to the z axis is defined by

$$\frac{n_x}{n_z} = \tan\beta = \pm\sqrt{\frac{\varepsilon_z(\varepsilon_y - \varepsilon_x)}{\varepsilon_x(\varepsilon_z - \varepsilon_y)}}. \tag{1}$$

We define the semi-angle A of the cone characterizing CD:

$$A = \frac{1}{n_y}\sqrt{(n_y - n_x)(n_z - n_y)}. \tag{2}$$

The emerging beam depends solely on the following variable [12]:

$$\rho_0 \equiv \frac{R_0}{w} = \frac{Al}{w}, \qquad \rho \equiv \frac{r}{w}, \tag{3}$$

with w the beam waist and the radius R_0 of the light cylinder dependent upon the angle A of the cone within the crystal and on the thickness l of the crystal: $R_0 = Al$.

In analogy to the terminology used for diffraction gratings [15], we define a "thin crystal" as a crystal generating a CD pattern with a parameter $\rho_0 \leq 1 \equiv w \geq R_0$. In this regime, the Poggendorff rings are not developed in opposition to a "thick crystal" ($\rho_0 \gg 1$), which generates fully developed Poggendorff rings. In the "thin crystal" regime, the output beam has a size similar to the input beam waist.

In practice, we use mainly lithium triborate (LiB_3O_5) or LBO. It is commonly used for frequency doubling in lasers, which makes it easy to get from multiple suppliers. As seen in Eq. (1), the binormal axis orientation of the crystal depends highly on the wavelength of the input beam. In the rest of this Letter, we will consider only the case of LBO; any other biaxial material (KTP, BiBO, $KNbO_3$, KGW, etc.) could be achromatized in the same way.

Considering the Sellmeier equations for an LBO crystal [16], we can calculate the variations of the different parameters of CD β and ρ_0. The dispersion of ρ_0 (due to variations of both

0146-9592/16/040769-04$15/0$15.00 © 2016 Optical Society of America

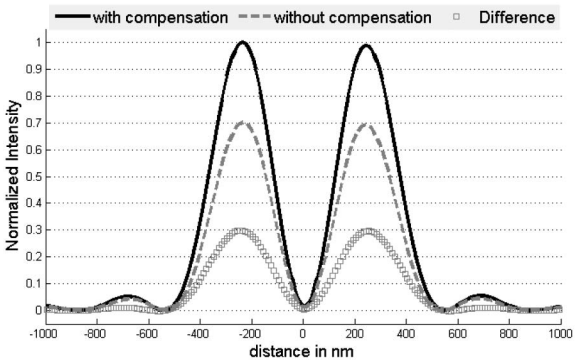

Fig. 1. Comparison of the profile of the vortex generated at $\lambda = 640$ nm with and without compensation of ρ_0 (reference set at $\lambda = 488$ nm). Only a difference in intensity can be found. The FWHM is the same for both distributions.

the semi-angle A and the beam waist w) could also be compensated, but is beyond the scope of this article, and thus, we will only deal with the direction of the binormal axis β. As a comparison, simulations for a given system geometry of a vortex beam at a wavelength $\lambda = 640$ nm with and without compensation of the dispersion of ρ_0 are presented in Fig. 1, showing that the absence of compensation of ρ_0 only influences the conversion efficiency of the phenomenon. The reference value $\rho_0 = 0.87$ is set at the one for $\lambda = 488$ nm, and the value of ρ_0 at $\lambda = 640$ nm without compensation is 0.65.

Figure 2 shows the dispersion of the orientation of the binormal axis for the LBO crystal between 400 and 650 nm. The maximal error on the orientation goes as high as 1°. This means that without compensation for this chromatic dispersion, it is impossible to generate an achromatic distribution of intensity on a range larger than several tens of nanometers as described, for example, by Berry and Jeffrey [17], even though LBO is found to be one of the least dispersive crystals suitable for CD.

To this end, we introduce a way to compensate this dispersion that involves the use of two custom-made right-angle prisms with the biaxial crystal in between them; the first one's dispersion exactly matches the one of the binormal axis, and the second one is redirecting the beam parallel to the geometrical axis of the system, but with a lateral shift, depending on the wavelength.

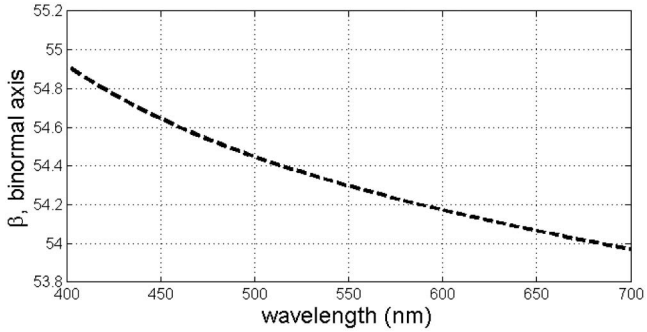

Fig. 2. Dispersion of the orientation of the binormal axis for the LBO crystal according to Eq. (1).

LBO has an Abbe number $V_{\mathrm{LBO}} = 63.97$, making it the equivalent to a crown glass (Abbe number $V > 50$). To compensate the dispersion of the binormal axis, we then use a flint glass. In order to reduce the angle of the prism, we chose to use a dense flint glass (H-ZF13 from CDGM Glass) which has an Abbe number $V_{H\text{-}ZF13} = 25.75$. A MATLAB routine enables us to optimize the prism angle for four propagation wavelengths (405, 488, 561, and 640 nm), corresponding to the usual fluorescence microscopy excitation wavelengths. The orientation of the binormal axis at 488 nm β_{488} is set as the reference axis and we assume that the crystal cut can be adjusted to match it. The differences ε_{λ_i} between the angle β_{λ_i} and β_{488} are given in Table 1.

The error between the orientation of β_{λ_i} as a function of the prism angle can be found in Fig. 3. Since an error of 0.1° is acceptable, the possible prism angle ranges roughly from 21° to 25°. However, in order to minimize the root mean square error defined as $\sigma_{\mathrm{RMS}} = (\varepsilon_{405}^2 + \varepsilon_{561}^2 + \varepsilon_{640}^2)^{1/2}$, the optimal value is found to be 23.155°.

A thorough simulation of a representative system (achromat focusing the beam followed by the designed crystal assembly) using ray-tracing software (Radiant OpticsStudio 14) enables us to double-check that the dispersion of the prism exactly matches the one of the binormal axis (Fig. 4). However, a lateral chromatic shift occurs when passing through the two prisms that needs to be compensated. We thus decided to insert the same prisms cemented together (without the crystal in between them) rotated by 180° to compensate for the lateral chromatic shift and bring back all the rays on the geometrical axis of the system, thus suppressing the need to decenter the following elements of the system (Fig. 4). Given the experimental conditions and especially the low F number the system works at ($F\sharp < F/15$) and the paraxiality, all other aberrations can be neglected. The in-focus spot diagram for both configurations (with and without lateral chromatic shift compensation prisms) are given in Fig. 4.

Table 1. Difference Between the Orientation of the Binormal Axis

$\varepsilon_{405} = \beta_{405} - \beta_{488}$	$\varepsilon_{561} = \beta_{561} - \beta_{488}$	$\varepsilon_{640} = \beta_{640} - \beta_{488}$
0.3981°	−0.2289°	−0.4200°

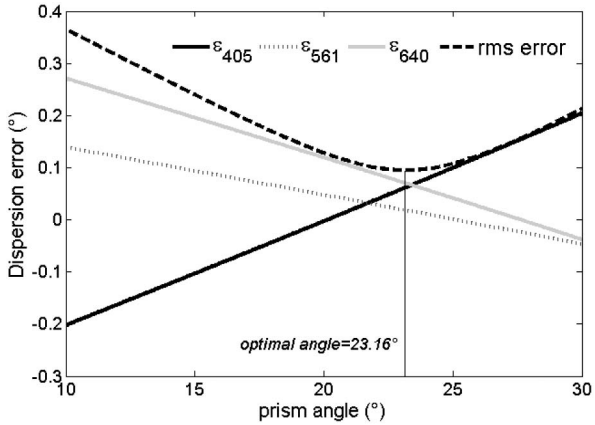

Fig. 3. Evolution of the binormal axis orientation error as a function of the prism angle.

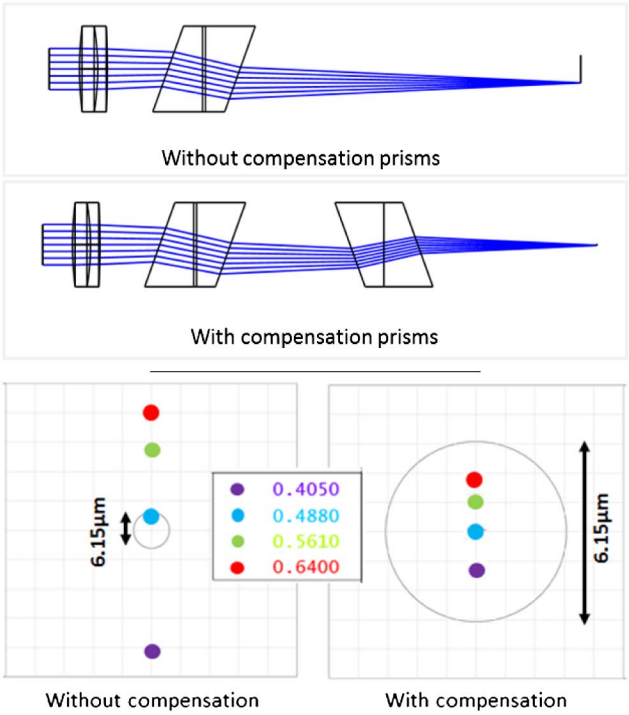

Fig. 4. Top: outlook of the simulated representative systems without compensation prisms and with compensation prisms; bottom: comparison between apochromatic arrangements without and with compensation prisms. Black circle indicates the corresponding Airy disk.

As demonstrated in [18], a simple three-element module (polarization state generator/biaxial crystal/polarization state analyzer) transforms a Gaussian beam into an optical vortex. The same kind of setup will be used for the experimental part of this article.

We now present the experimental results obtained with the achromatic biaxial crystal. A laser combiner (MLE-LFA, Toptica) with four wavelengths (405, 488, 561, and 640 nm) with a fiber output is fed to a reflective collimator (RC04APC-P01, Thorlabs) to generate a 4 mm collimated beam. The linear 0° polarization of the beam is improved by a broadband polarizing beam splitter (PBS) (CM1-PBS251, Thorlabs), and a variable retarder (VPR, Arcoptix) with its fast axis oriented at 45° enables the generation of an elliptical polarization with its azimuth at 0° or 90° and an ellipticity from −45° to 45°. This beam is then focused by an achromat $f' = 75$ mm (32–882, Edmund Optics); it then passes through the custom-made achromatic "thin crystal" of 0.5 mm with a compensation for the lateral chromatic shift with a numerical aperture $\mathrm{NA} = 2/75 = 0.027$ ($\rho_0 = 0.87$ for $\lambda = 488$ nm), the same achromat in the reverse orientation recollimates the beam. It needs to be noted that the axial position of the crystal assembly does not impact CD, since the effect only depends on the angles and not the position of the crystal. Another variable retarder (VPR, Arcoptix), with its fast axis oriented at 45° coupled to a second PBS, acts as a polarization state analyzer. The beam is then focused by a third achromat $f' = 30$ mm (32–313, Edmund Optics) on a monochrome CCD camera (Atik 314L+). A sketch of the experimental setup can be found in Fig. 5.

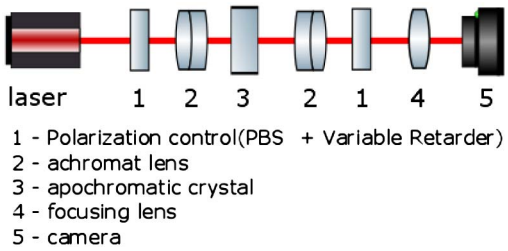

Fig. 5. Experimental setup used to generate the data provided in this Letter.

Also, as seen in [18–20], CD enables the easy generation of a vector beam that resembles the usual Laguerre–Gauss mode LG_{01} for a circularly polarized input beam, whereas, when using a linearly polarized input beam, the beam acquires a modulation that resembles the Hermite–Gauss HG_{01} mode (assuming a horizontal linear polarization input and assuming that the crystal crystallographic axes are aligned with the Cartesian coordinates system). Previous attempts to generate white light CD distributions [21] were only aiming at theoretically describing the dependency on the wavelength of CD. The intensity distributions obtained with the thick crystal clearly showed that the Poggendorff rings could only be generated in a small spectral range, since CD is quickly evolving to double refraction. We present here the first implementation of an optical vortex in white light by CD. We used the same experimental setup as described previously, with the same wavelengths, namely, 405, 488, 561, and 640 nm (see Fig. 6). The input and output states of polarization are set to circular ones by adapting the voltage applied to the variable retarder to reach a quarter-wave retardation. Since the voltage required to reach a circular polarization differs for each wavelength, images have been acquired independently and later combined in a single multichannel image without any registration.

We define the following metrics to estimate the vortex beam quality:

$$\begin{array}{c|l} \text{symmetry}(\%) & S = I_{\text{peak},1}/I_{\text{peak},2} \\ \text{Contrast}(\%) & C = (I_{\text{peak}} - I_{\min})/(I_{\text{peak}} + I_{\min}). \end{array} \tag{4}$$

Results are compiled in Table 2.

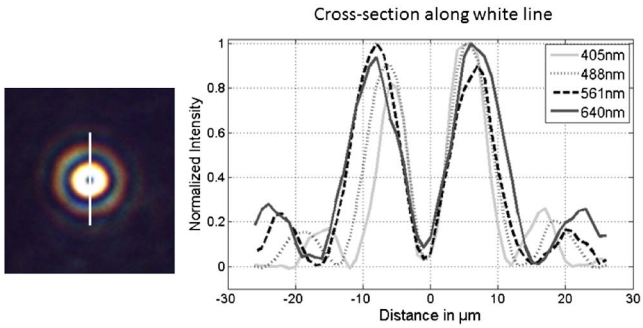

Fig. 6. Left: experimental achromatic vortex (circularly polarized input Gaussian beam) generated by CD in the apochromatic crystal arrangement imaged on a gray-level CCD camera at 405, 488, 561, and 640 nm (one wavelength at a time); right: cross-section along the white line.

Table 2. Vortex Beam Quality Estimators

λ (nm)	405	488	561	640
S (%)	82.5	90.6	80.0	94.0
C (%)	93.6	95.0	92.5	84.0
D (peak to peak) (μm)	11.5	12	13.5	14

Table 3. Pseudo Hermite–Gauss Mode Quality Estimators

λ (nm)	405	488	561	640
S (%)	94.0	85.6	93.0	82.7
C (%)	92.5	90.58	93.31	91.37
D (min to min) (μm)	8	9	9	9

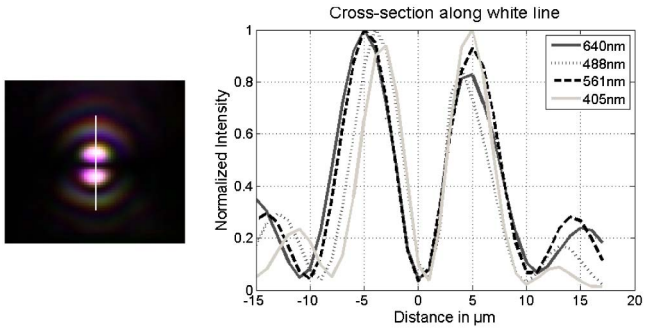

Fig. 7. Pseudo Hermite–Gauss modes (linearly polarized Gaussian input beam) generated by CD in the apochromatic crystal arrangement imaged on a gray-level CCD camera at 405, 488, 561, and 640 nm (one wavelength at a time); right: cross-section along the white line.

A close inspection of the estimators show that the distance between the two maxima (D) is not proportional to the wavelength, which clearly indicates an experimental problem. We can also notice that the symmetry and contrast vary highly with the wavelength. We suspect a polarization control issue, especially errors on the voltage applied to the liquid-crystal variable retarder, which induce an ellipticity error, ultimately leading to a deviation from the vortex. To confirm this hypothesis, the variable retarders are removed, leaving only the PBS in the beam path. The obtained images are shown in Fig. 7.

The compensated apochromatic crystal arrangement enables the generation of Hermite–Gauss modes on a wide wavelength range from 405 to 640 nm between crossed linear polarizers. As seen on the stack image, all the distributions are co-localized without any registration, and the black line in the center is well preserved. A look at the calculated estimators (see Table 3) shows that the symmetry and the contrast have been vastly improved, though the distance between the lobes still is not proportional to the wavelength, the distributions having the same size no matter the wavelength. It is confirmed that a better polarization control based on achromatic elements and improved lateral and axial chromatism correction would lead to close to perfect generation of an achromatic vortex beam, which has not, to the authors' best knowledge, been achieved yet.

We have demonstrated here both theoretically and experimentally a method to compensate the dispersion of the direction of the binormal axis of a biaxial crystal for CD by inserting the crystal between two right-angle prisms. This geometry enables the simple and robust generation of white-light (spectral band between 405 and 640 nm) achromatic optical vortices that only depend on the quality of the polarization elements to control the states of polarization of the input and output beams. The efficiency (defined as the percentage of light converted into a vortex) of this process can be made to reach more than 75% by adjustment of the crystal parameters. This technique could prove extremely useful for superresolution microscopy (e.g., STED microscopy), especially for systems using a supercontinuum as depletion. Though presented in the visible range (405–640 nm range) for a thin crystal, this simple concept can be easily extended to a more suitable range for STED microscopy (550–800 nm), or to higher thicknesses of crystal to generate the well-known Poggendorff rings of CD.

REFERENCES

1. K. T. Gahagan and G. A. Swartzlander, Opt. Lett. **21**, 827 (1996).
2. T. A. Klar, E. Engel, and S. W. Hell, Phys. Rev. E **64**, 066613 (2001).
3. M. Beijersbergen, R. Coerwinkel, M. Kristensen, and J. Woerdman, Opt. Commun. **112**, 321 (1994).
4. N. R. Heckenberg, R. McDuff, C. P. Smith, and A. G. White, Opt Lett **17**, 221 (1992).
5. G. A. Swartzlander, Opt. Lett. **31**, 2042 (2006).
6. W. W. R. Hamilton, Trans. R. Irish Acad. **17**, 1 (1837).
7. D. P. O'Dwyer, K. E. Ballantine, C. F. Phelan, J. G. Lunney, and J. F. Donegan, Opt. Express **20**, 21119 (2012).
8. A. Abdolvand, K. G. Wilcox, T. K. Kalkandjiev, and E. U. Rafailov, Opt. Express **18**, 2753 (2010).
9. A. Peinado, A. Lizana, A. Turpín, C. Iemmi, K. Todor, J. Mompart, and J. Campos, Opt. Express **23**, 5453 (2015).
10. S. Rosen, G. G. Y. Sirat, H. Ilan, and A. J. A. Agranat, Opt. Express **21**, 10133 (2013).
11. J. Caron, C. Fallet, J.-Y. Tinevez, L. Moisan, L. P. Braitbart, G. Y. Sirat, and S. L. Shorte, Cell Adhes. **8**, 430 (2014).
12. M. V. Berry, J. Opt. A **6**, 289 (2004).
13. M. V. Berry, M. R. Jeffrey, and J. G. Lunney, Proc. R. Soc. A **462**, 1629 (2006).
14. A. Belskii and A. Khalpalyuk, Opt. Spectrosc. **44**, 436 (1978).
15. T. K. Gaylord and M. G. Moharam, Appl. Opt. **20**, 3271 (1981).
16. C. Chen, Y. Wu, A. Jiang, B. Wu, G. You, R. Li, and S. Lin, J. Opt. Soc. Am. B **6**, 616 (1989).
17. M. V. Berry and M. R. Jeffrey, J. Opt. A **8**, 1043 (2006).
18. V. Peet, Proc. SPIE **8429**, 842914 (2012).
19. C. F. Phelan, J. F. Donegan, and J. G. Lunney, Opt. Express **19**, 21793 (2011).
20. A. Turpin, Y. V. Loiko, A. Peinado, A. Lizana, T. K. Kalkandjiev, J. Campos, and J. Mompart, Opt. Express **23**, 5704 (2015).
21. R. T. Darcy, D. McCloskey, K. E. Ballantine, B. D. Jennings, J. G. Lunney, P. R. Eastham, and J. F. Donegan, Opt. Express **21**, 20394 (2013).